



Analysis of temperature and frequency dependent dielectric properties, dynamic hysteresis loop and thermal energy conversion in $\text{BaZr}_{0.05}\text{Ti}_{0.95}\text{O}_3$ ceramic

G. Nag Bhargavi¹ · Ayush Khare¹ · T. Badapanda² · M. S. Anwar³ · Nameeta Brahme⁴

Received: 30 January 2018 / Accepted: 3 May 2018 / Published online: 8 May 2018
© Springer Science+Business Media, LLC, part of Springer Nature 2018

Abstract

The barium zirconium titanate ceramic with formula $\text{BaZr}_{0.05}\text{Ti}_{0.95}\text{O}_3$ has been synthesized by the conventional solid state reaction technique. The synthesized ceramic sample is characterized by X-ray diffraction, scanning electron microscopy, Raman spectroscopy, temperature dependent dielectric spectroscopy and ferroelectric behaviour. The Raman spectrum confirms the orthorhombic structure at room temperature and local distortions due to distorted octahedral structures. The temperature dependent dielectric study reveals the occurrence of three transition temperatures representing rhombohedra to orthorhombic, orthorhombic to tetragonal and tetragonal to cubic transition in the material. The area of the hysteresis loop decreases with temperature up to the transition temperature, followed by an increase at higher temperatures. Scaling relations for coercive field (E_c) and remnant polarization (P_r) are studied as a function of temperature. This exhibits back-switching polarization behaviour as a function of temperature. The thermal energy conversion potential of the studied sample is obtained by using Olsen cycle.

1 Introduction

Ferroelectric materials are widely used due to their excellent properties, such as hysteresis (non-volatile memory), high piezoelectric effect (actuators), strong electro-optic effect (electro-optic materials for data storage applications), high dielectric constant (capacitors), high pyro-electric coefficient (infrared detectors), high dielectric constant and anomalous temperature coefficient of resistivity [1–9]. Most of the work on the ferroelectric materials has been based on lead based materials, but due to environmental concern, they are not found suitable for direct industrial applications [10–13]. Recently, certain lead free perovskites are extensively

studied due to their extraordinary dielectric, ferroelectric, piezoelectric, strain and electrostrictive properties. Among others, BaTiO_3 (BT) has attracted most of the attention due to its high dielectric constant, and ferroelectric behaviour for practical applications [14–19]. But, BT ceramic offers three main disadvantages. First, it has tetragonal to orthorhombic phase transition below room temperature ($\sim 5^\circ\text{C}$); secondly, in the tetragonal phase the resonant frequency rises rapidly with temperature, and third is high dielectric loss shown by it. In order to overcome the drawbacks along with improvement in various properties, BT system needs to be modified. It has been reported that incorporation of Zr^{4+} ions in BaTiO_3 [$\text{BaZr}_x\text{Ti}_{(1-x)}\text{O}_3$] improves its properties, and shifts the Curie temperature towards lower side as Zr^{4+} is chemically more stable than Ti^{4+} . Also, the feasibility of substitution of Ti^{4+} ions by Zr^{4+} ions lies in the fact that Zr^{4+} having larger ionic radius expands the lattice structure that reduces the possibility of conduction by electron hopping between Ti^{4+} and Ti^{3+} ions [20–29]. An interesting observation on the BZT system (with $x=0.05$) was reported earlier, which exhibited high piezoelectric coefficient ($d_{33}=236$ pC/N) and electromechanical coupling factor ($K_{33}=56.5\%$) [30]. Recently, a high value of d_{33} i.e., 300 pC/N (420 pC/N, $k_p=49\%$ at 100 h sintering time) was reported for composition with $x=0.06$ [31]. Kalyani et al. have reported that

✉ Ayush Khare
akhare.phy@nitrr.ac.in

¹ Department of Physics, National Institute of Technology, Raipur 492010, India

² Department of Physics, C.V. Raman College of Engineering, Bhubaneswar 752054, India

³ Colloids & Materials Chemistry, Institute of Minerals and Materials Technology, Bhubaneswar 751013, India

⁴ School of Studies in Physics and Astrophysics, Pt. Ravishankar Shukla University, Raipur 492010, India

$\text{BaZr}_{0.05}\text{Ti}_{0.95}\text{O}_3$ showed high piezoelectric properties due to existence of morphotropic phase boundary [32].

A systematic literature survey suggests that $\text{BaZr}_{0.05}\text{Ti}_{0.95}\text{O}_3$ shows good dielectric, ferroelectric and piezoelectric behaviour. Even though, there are few reports on the dielectric, ferroelectric and piezoelectric study on the composition reported in this paper, but the effect of temperature on the dielectric and ferroelectric behaviour has not been reported yet. The results of electrical characterizations of $\text{BaZr}_{0.05}\text{Ti}_{0.95}\text{O}_3$ ceramic presented in our earlier publication [24] are quite encouraging and this has motivated us to further undertake the temperature and frequency dependent dielectric properties on $\text{BaZr}_{0.05}\text{Ti}_{0.95}\text{O}_3$ ceramic. The present manuscript is focused on the temperature dependent dielectric, dynamic hysteresis and thermal energy conversion analyses of $\text{BaZr}_{0.05}\text{Ti}_{0.95}\text{O}_3$ ceramic. In order to understand the effect of temperature on the ferroelectric properties, hysteresis scaling relations of coercive field and remnant polarization as a function of temperature have been systematically studied and discussed. Additionally, back switching polarization behaviour as a function of temperature is estimated by well established Arrhenius law and, average values of activation energy are evaluated. The novelty of the paper lies in the facts that the scaling relations for coercive field and polarization, and thermal energy conversion of the material are being reported for the first time.

2 Experimental techniques

2.1 Synthesis

The $\text{Ba}(\text{Zr}_{0.05}\text{Ti}_{0.95})\text{O}_3$ (BZT) ceramic powder was synthesized by the conventional high temperature solid state reaction technique (SSR). The particulars of the precursors used and the various steps involved in the process of synthesis have been discussed in detail in our earlier report [24].

2.2 Characterizations

The crystal structure and phase purity of the synthesized powder was characterized by means of X-ray diffraction (XRD) using Panalytical X'pert Pro diffractometer operated by specific $\text{Cu K}\alpha$ radiation having wavelength, $\lambda = 1.541 \text{ \AA}$. The X-ray analysis was carried in the 2θ range of $10^\circ \leq 2\theta \leq 90^\circ$ and at a scanning rate of $2^\circ/\text{min}$. The surface morphological study was done by the help of Zeiss (Germany) make scanning electron microscopy (SEM) using gold as conducting surface. The structural changes and disorder in the ceramic sample were studied in terms of Raman spectra, and data was collected in the range from 100 to 1000 cm^{-1} using Jobin Yvon Horiba, France make spectrometer (Model T64000) with Argon–Krypton mixed ion

gas laser (Model 2018 RM). The dielectric measurements were performed in the temperature range from 80 to 500 K and at different frequencies using Hioki, Japan make LCR tester connected to a computer. The ferroelectric behaviour was explored by using Marine India make P–E loop tracer at different temperatures.

3 Results and discussion

3.1 X-ray diffraction (XRD) and scanning electron microscopy (SEM)

The phase formation of the $\text{BaZr}_{0.05}\text{Ti}_{0.95}\text{O}_3$ powder was confirmed by the XRD performed at room temperature. The details of the results of XRD studies are reported in our earlier article [24]. The SEM micrograph of the $\text{BaZr}_{0.05}\text{Ti}_{0.95}\text{O}_3$ ceramic taken at a magnification of 3.00 K shows well densified grains with an average grain size of $10 \mu\text{m}$ as reported earlier [24]. The similar kind of ferroelectric domains with lamellar structures were reported by Serrano et al. [33] and Tan et al. [34] in BZT and BaTiO_3 ceramics, respectively.

3.2 Raman spectroscopic studies

Raman spectroscopy is an appropriate tool to get more insight into the local distortions, disorder and the strain present in the system. Figure 1 displays the room temperature Raman spectrum of $\text{BaZr}_{0.05}\text{Ti}_{0.95}\text{O}_3$ ceramic powder in the wave number range from 100 to 1000 cm^{-1} . The Raman active modes of phonons are recorded at different frequencies. The important features appeared in the spectrum are: (i) intense and broad band at 522 cm^{-1} [$A_1(\text{TO})$] and 282 cm^{-1} [$A_1(\text{TO})$] (ii) broad and less intense peak at 717 cm^{-1} [$A_1(\text{LO})$], (iii) sharp band at 305 cm^{-1} [$B_1, E(\text{TO} + \text{LO})$] (iv) a weak band at 185.8 cm^{-1} [$A_1(\text{LO})$] represents orthorhombic phase at room temperature, and (v) asymmetric peak at 516 cm^{-1} [$A_1(\text{TO})$] suggests the existence of coupling of TO modes associated with the tetragonal phase [35–37]. The A(LO) mode at 720 cm^{-1} represents the addition of Zr to BaTiO_3 , which leads to substitution of Ti ions [38, 39]. The 305 cm^{-1} phonon mode represents local distortion in the octahedral ($\text{TiO}_6/\text{ZrO}_6$) clusters [35].

3.3 Temperature and frequency dependence of dielectric constant

Figure 2a presents the dielectric behaviour of the BZT ceramic as a function of temperature at various frequencies (1, 10, 100, 500 kHz and 1 MHz). For all the frequencies, as noticed from figure, the dielectric constant (ϵ) first increases gradually to its maximum value (ϵ_m) and then

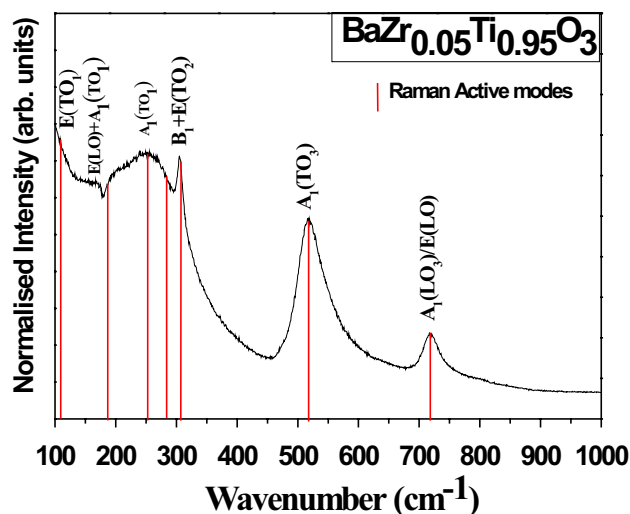


Fig. 1 Raman spectrum of $\text{BaZr}_{0.05}\text{Ti}_{0.95}\text{O}_3$ ceramic calcined at $1200\text{ }^\circ\text{C}$ for 4 h. The vertical lines (red) indicate the Raman active modes. (Color figure online)

decreases smoothly with increase in temperature representing the phase transition temperature. The graph depicts three structural phase transitions at 400 K (T_c), 339 K (T_1) and 300 K (T_2). The sharp peak at 400 K (Curie temperature) represents the transition temperature (T_c), which is associated with ferroelectric (tetragonal) to paraelectric (cubic) phase transition. It is also observed that the maximum value of dielectric constant (ϵ_m) decreases with frequency due to the merging of all kind of polarizations at higher frequencies. A small hump is observed around 339 K (T_1) indicating orthorhombic to tetragonal transition or ferroelectric to ferroelectric transition. A third peak observed at 300 K is due to rhombohedral to orthorhombic phase transition. The dielectric study confirms the existence of orthorhombic structure of the material at room temperature also. A comparison of our results with other reported results validate the findings reported in this article [40].

The frequency dependence of dielectric constant in the temperature range from 40 to $150\text{ }^\circ\text{C}$ is plotted in Fig. 2b. Initially, the dielectric constant is high at lower frequencies, and is found to decrease with increasing frequency at all the temperatures. The higher value of dielectric constant at lower frequencies is attributed to the excitation of bound electrons, lattice vibration, dipole orientation and space charge polarization (electronic, atomic, interfacial and ionic, etc.). As frequencies increase, various mechanisms cease to contribute to the total polarizability resulting in diminution in dielectric constant. At higher frequencies, relative permittivity becomes almost constant showing frequency independent behaviour. This can be understood from Maxwell–Wagner type polarization and

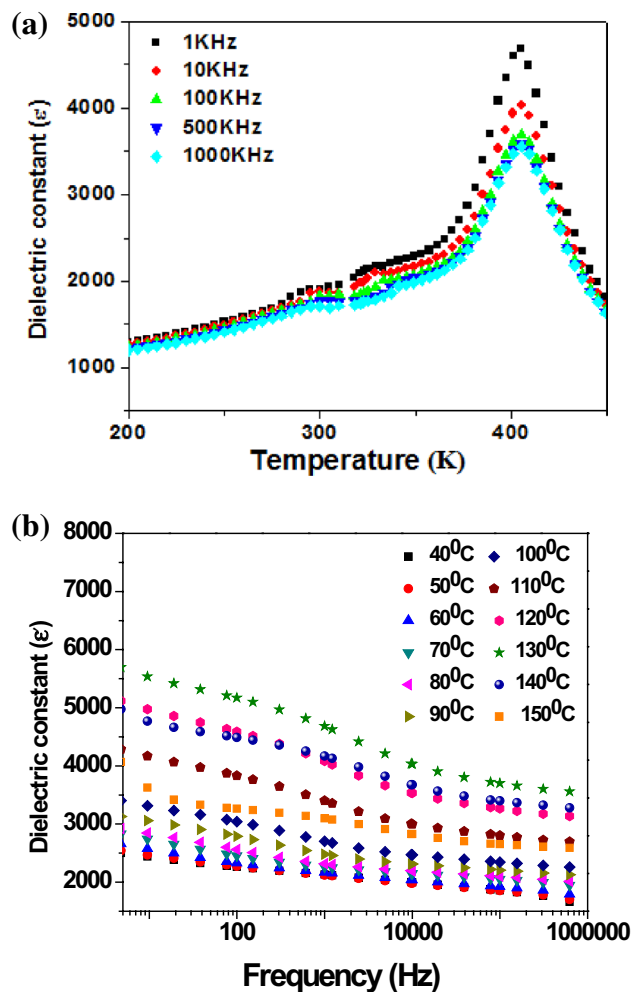


Fig. 2 **a** Variation in dielectric constant with temperature for $\text{BaZr}_{0.05}\text{Ti}_{0.95}\text{O}_3$ ceramic at various frequencies. **b** Variation in dielectric constant with frequency for $\text{BaZr}_{0.05}\text{Ti}_{0.95}\text{O}_3$ ceramic at various temperatures

Koop's phenomenological theory of dielectrics [41, 42]. In the low frequency region, electric dipoles follow the frequency of applied field, but in the high frequency region the electric dipoles can not follow the fast variations of the applied field [43], and hence the values of ϵ remain constant. Figure 2b also shows that for a particular frequency the dielectric constant increases with increase in temperature up to $130\text{ }^\circ\text{C}$ (near Curie temperature) followed by decrease at still higher temperatures. The variation of ϵ with temperature is different for non-polar and polar polymers. In general, for non-polar polymers, ϵ is independent of temperature. However, in the case of polar polymers, the dielectric permittivity increases with increasing temperature [44]. This behaviour of polar dielectrics is typical because dipole orientation is facilitated by increasing temperature, thus increasing the permittivity.

3.4 Temperature and frequency dependence of dielectric loss

The dielectric loss ($\tan\delta$) is an important factor, which determines the suitability of a material in microelectronic systems. The dielectric loss results from several mechanisms: (1) ion migration; (2) ion vibration and deformation; (3) electronic polarization, etc. The most important mechanism applicable to most of the ceramics is ion migration. Ion migration is strongly affected by temperature and frequency. The losses due to ion migration are dominating at lower frequencies and temperatures [45]. The variation of dielectric loss with temperature at various frequencies (1 kHz–1 MHz) is shown in Fig. 3a. The plot depicts dispersion of $\tan\delta$ at lower frequencies; however, no peaks are observed in the dielectric loss factor in the middle of temperature region. Unlike previous case, the dielectric loss is almost constant

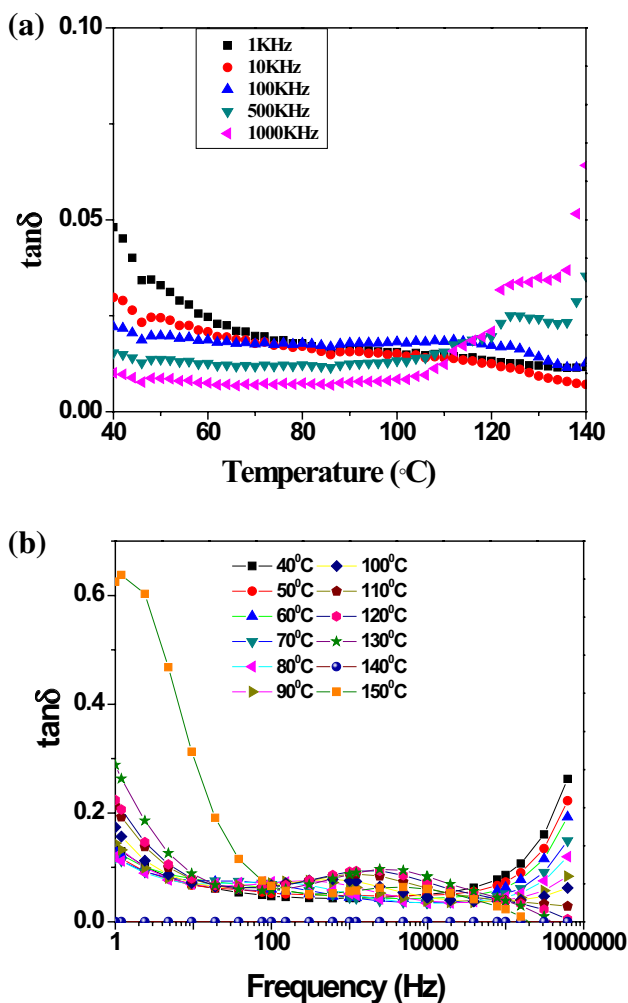


Fig. 3 a Variation in dielectric loss with temperature for $\text{BaZr}_{0.05}\text{Ti}_{0.95}\text{O}_3$ ceramic at various frequencies. b Variation in dielectric loss with frequency for $\text{BaZr}_{0.05}\text{Ti}_{0.95}\text{O}_3$ ceramic at various temperatures

up to 130 °C for all the frequencies. At higher temperatures (above 130 °C), the dielectric loss rapidly increases. This is due to the leakage conductivity, which has a significant effect on dielectric loss at higher temperatures [46]. Figure 3b shows the variation of dielectric loss as a function of frequency at different temperatures (from 40 to 150 °C). As is evident from the figure, the dielectric loss is very less (almost < 1) for all the temperatures and frequencies. The dielectric loss of the sample is very less for temperatures below 130 °C (ferroelectric phase), but its value is found to increase rapidly in the paraelectric phase (above 130 °C).

3.5 Diffusivity analysis

The diffuseness of the phase transition is given by the modified Curie–Weiss law as:

$$\frac{1}{\epsilon'} - \frac{1}{\epsilon_m} = (T - T_m)^\gamma / C' \tag{1}$$

where γ and C' are constants. γ is the parameter, which gives idea about the nature of the phase transition. $\gamma = 1$ indicates normal ferroelectric behaviour, while $\gamma = 2$ tells diffused (relaxor like) phase transition. A plot between $\log(1/\epsilon' - 1/\epsilon_m)$ and $\log(T - T_m)$ at 100 kHz frequency is presented in Fig. 4, which follows Curie–Weiss law, and a close linear relationship is observed. In the present study, the value of γ is found to be 1.45, which tends towards the diffuse ferroelectric behaviour. The broadness or diffusiveness occurs mainly due to compositional fluctuation and structural disordering in the arrangement of cation at one or more crystallographic sites of the structure. Hence, Ti^{4+} cations can stabilize the normal ferroelectrics phase in BT, while Zr^{4+} cations at B-sites behave as a typical destabilizer against

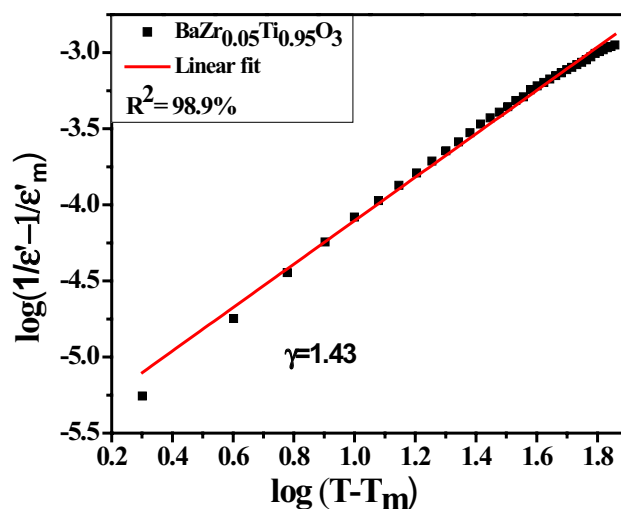


Fig. 4 Plot of $\log(1/\epsilon' - 1/\epsilon_m)$ versus $\log(T - T_m)$ for $\text{BaZr}_{0.05}\text{Ti}_{0.95}\text{O}_3$ ceramic at 100 kHz frequency

normal ferroelectrics and induce paraelectric behaviour due to their higher ionic diameter and lower polarization. When Zr ions are doped in to BaTiO₃ matrix, more and more macro-domains (long-range ordered regions) break up into micropolar regions transforming from the normal ferroelectrics to the diffuse ferroelectric phase due to the larger ionic diameter of Zr ions [47]. As a result, a compositionally more disordered state appears, and the ferroelectric phase transition becomes smeared out by the chemical inhomogeneity leading to enhancement in diffuseness.

3.6 Temperature dependent ferroelectric studies

In order to investigate the ferroelectric properties of BZT ceramic, the measurement of polarization as a function of electric field (P–E hysteresis loop) is carried out. Figure 5a illustrates the P–E hysteresis loop of BZT ceramic at 9 kV/cm electric field and elevated temperatures ranging from 30 to 150 °C. Figure 5b shows the variation of remanent

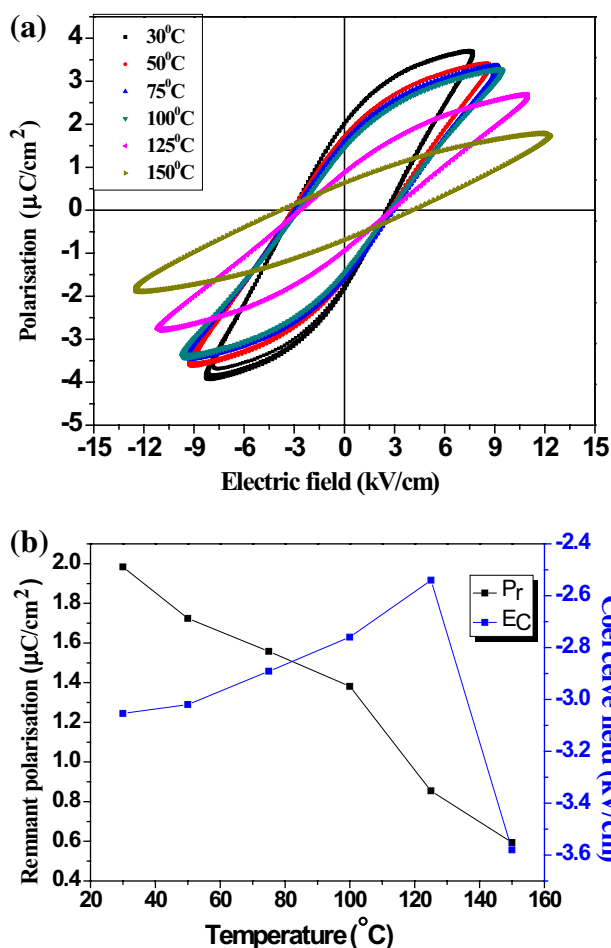


Fig. 5 a P–E loop of for BaZr_{0.05}Ti_{0.95}O₃ ceramic at various temperatures. b Variation of remanent polarization with temperature (P_r remanent polarization, E_c coercive field)

polarization (P_r) and coercive field (E_c) with temperature. Remanent polarization and coercive fields decrease with increasing temperature. This may result due to the effect of thermal fluctuations on the ferroelectric interaction among the dipoles and the lattice distortion [48] and decreasing P_r values. It is also observed from the plot (Fig. 5b) that the coercive fields decrease up to the 125 °C followed by increase thereafter indicating that the transition temperature is close to 125 °C. It can be seen that the area of the loop decreases with rising temperature. Here, it is important to mention that loop area is related to domain wall motion, and larger area at lower temperature implies the increase of difficulty for domain wall motion and with an increasing temperature, the area of the loops decreases and becomes unsaturated [49]. Again, it is observed that there is still some polarization beyond the transition temperature.

Hysteresis loop is a common feature of a ferroelectric material. It basically represents the difference in energy required during polarization and depolarization of the ferroelectric material in the form of heat. The heat absorbed during this process can be converted into electricity. It is reported that the polarization in reverse order can be traced into a clockwise loop between two temperatures. This cycle is known as Olsen cycle, which converts thermal energy into electricity. The Olsen cycle has two important features: (i) two isothermal and (ii) two isoelectric field processes [50, 51]. The cycle 1→2→3→4→1 shown in Fig. 6 is the electric analog of Olsen cycle and the area under the closed cycle gives electric energy produced per unit volume per cycle. Various reports are available on the details of the Olsen cycle [52–54]. In the cycle, the process 1→2 is a constant low temperature (T_L) part, where the electric field increases from lower limit E_L to higher limit E_H . In this process, the material polarization increases. In the

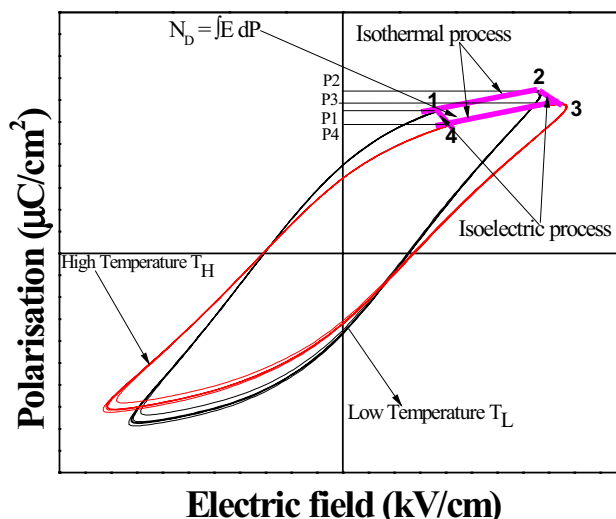


Fig. 6 Schematic diagram showing electrical energy conversion using Olsen cycle for BaZr_{0.05}Ti_{0.95}O₃ ceramic

process 2→3, heat is supplied to the material, which increases its temperature, produces lattice vibrations and the material depolarizes at constant electric field E_H . In this process, the temperature jumps from T_L to T_H . This results in generation of large depolarization current that can be stored for powering electronic equipment using suitable circuit. The process 3→4 is again a constant temperature process, where electric field reduces from E_H to E_L . As the electric field decreases, the polarization decreases due to which a weak polarization current develops. Finally, in the process 4→1, heat is extracted from the system at constant electric field (E_L) and that the material returns to its initial state, and cycle is completed. The energy density per unit volume of the sample can mathematically be expressed as [55]:

$$N_D = \oint E dP \quad (2)$$

where E and P are electric field and polarization, respectively. The Olsen cycle is employed for BZT ceramic in the

temperature range 30–125 °C. The cycle is operated at a voltage of 9 kV/cm and T_L is kept 30 °C. The energy conversion based on Olsen cycle for BZT ceramic as a function of applied higher electric field (E_H) at higher temperature (T_H) is shown in Fig. 7a–d. From the plots, it is observed that as the temperature difference increases, energy increases. Upon operating the cycle between 30 and 125 °C at 9 kV/cm, the maximum energy is calculated as 4.25 kJ/m³. The values of energy calculated in different temperature ranges are summarized in Table 1.

Table 1 Values of energy calculated in different temperature ranges

T_L-T_H (°C)	ΔT (°C)	E_L-E_H (kV/cm)	ΔE (kV/cm)	ΔW (kJ/m ³)
30–50	20	3.25–7.41	4.16	1.25
30–75	45	3.25–7.43	4.18	1.3
30–100	70	3.25–7.4	4.15	1.91
30–125	95	3.25–7.42	4.17	4.25

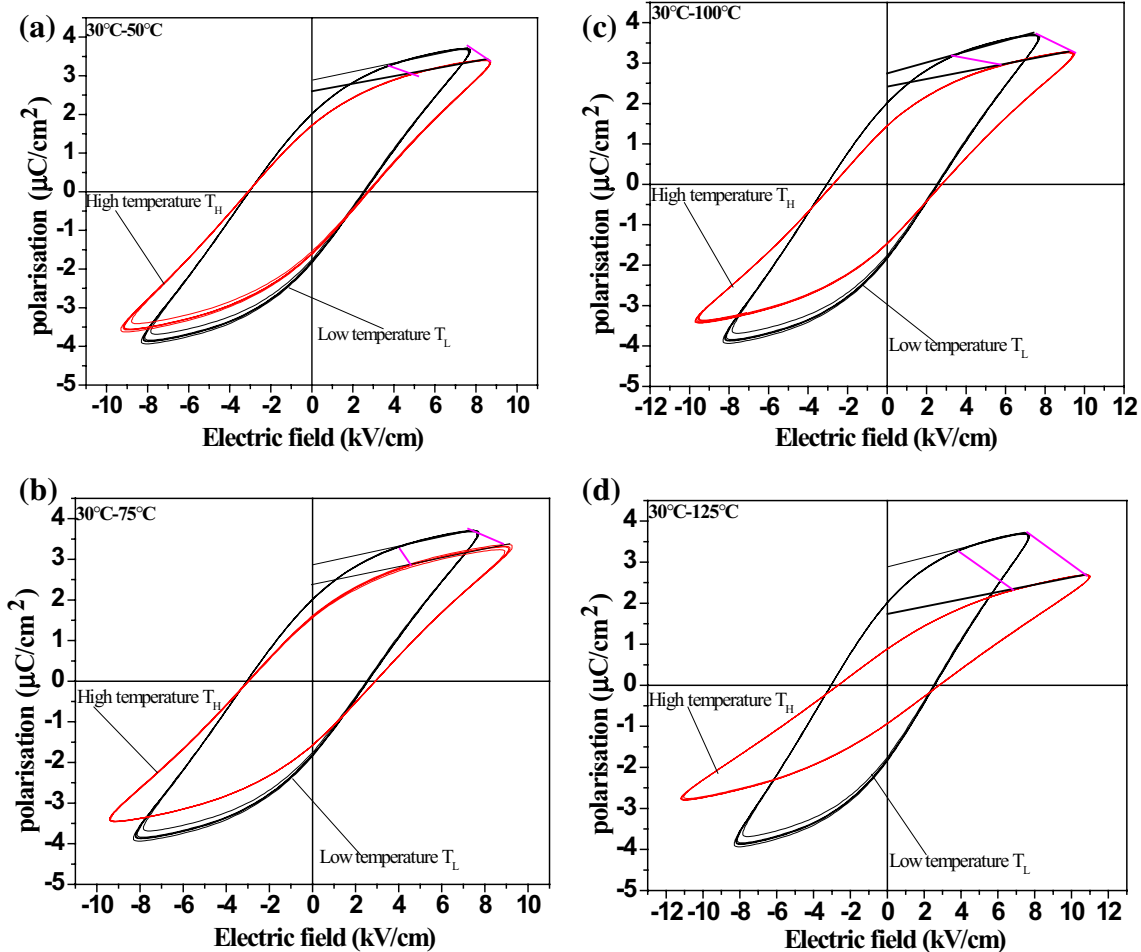


Fig. 7 a–d Olsen cycle for BaZr_{0.05}Ti_{0.95}O₃ ceramic at various temperature differences: **a** 30–50 °C, **b** 30–75 °C, **c** 30–100 °C, **d** 30–125 °C

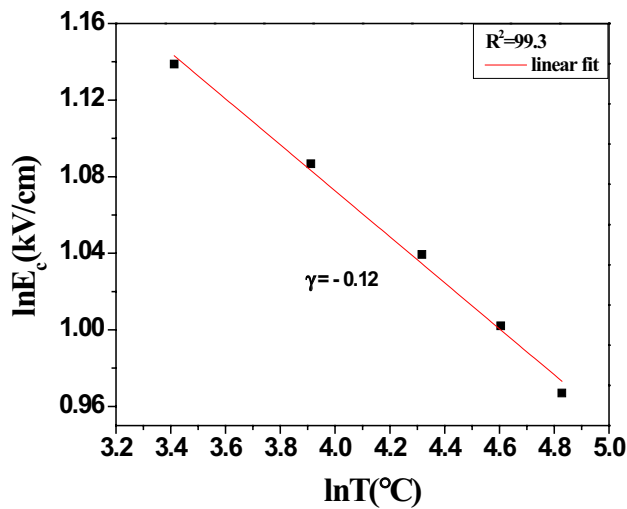


Fig. 8 Logarithmic plot of coercive field (E_c) with temperature (T) at 9 kV/cm electric field

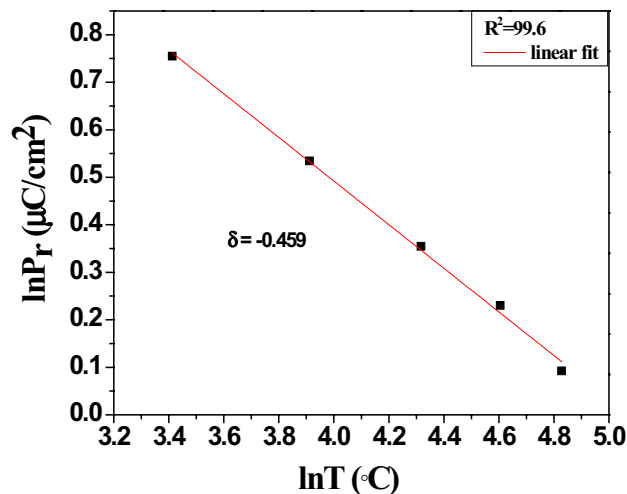


Fig. 9 Logarithmic plot of remanent polarization (P_r) with temperature (T) at 9 kV/cm electric field

The variation of hysteresis loop parameters with temperature and electric field are also studied. For this, the P–E loop parameters coercive field (E_c) and remanent polarization (P_r) are plotted against temperature (T). The plots of $\ln E_c$ versus $\ln T$ and $\ln P_r$ versus $\ln T$ at 9 kV/cm electric field are presented in Figs. 8 and 9, respectively. The dependence of $\ln E_c$ on $\ln T$ was studied in terms of linear least square fitting method. Linear least squares is an approach to fitting a mathematical or statistical model to data in cases where the idealized value provided by the model for any data point is expressed linearly in terms of the unknown parameters of the model. In the present case, the fitting parameter was found to be $R^2 \sim 0.993$, which is quite acceptable when compared with ideal value. The slope (γ) of the graph ($\ln E_c$ vs. $\log T$)

gives the scaling relationship between E_c and T . A linear relationship between E_c and T is mathematically expressed in terms of following linear equation:

$$\ln E_c = \gamma \ln T + Y_{Ec} \quad (3)$$

where γ is the slope of the plot and Y_{Ec} is the Y- intercept. In the present study, the experimental values obtained from different studies satisfy Eq. (3) very well. In Eq. (3), Y_{Ec} (Y-intercept) plays a key role in determining the value of E_c at 0 °C temperature but the theoretical value of E_c estimated from Y intercept of the graph may differ from experimental values. It is because at 0 °C, all the ferroelectric domains become frozen and, it is expected that ferroelectric properties deviate from their normal behaviour at high temperatures.

Similar studies were performed on $\ln P_r$ versus $\ln T$ plot at 9 kV/cm electric field which is shown in Fig. 9. Mathematically, the plot can be expressed by the equation:

$$\ln P_r = \delta \ln T + Y_{Pr} \quad (4)$$

where δ is the slope of the plot and Y_{Pr} is the Y- intercept.

In this study also, the obtained experimental values are in accordance with Eq. (4) and value of slope δ is supported by theoretical results. The scaling relationship between E_c and P_r with temperature at different electric fields can be explained on the basis of ferroelectric domain switching [56–60]. Ferroelectric domain switching is the process when the dipoles change from one spontaneously polarised state to the other by applied electric field. The domain switching is a regular phenomenon in all the ferroelectric materials, but the behaviour can be different for different compositions at morphotropic phase boundaries, crystal structure, doping, defects and domain states. The phenomenon of switching of domains is attributed to two mechanisms: one is domain wall motion and other is nucleation of domains. At lower electric fields, the nucleation is slow which dominates the switching process, while at higher electric fields the domain wall switching is feasible and the dipoles orient in the direction of electric field. As the electric field increases, the area of hysteresis loop increases and attains its saturation value. The domain wall motion is greatly influenced by temperature because the rise in temperature increases the lattice vibrations due to which the orientation of dipoles increases, which reduces the stability of polarization. Hence, the hysteresis loop area decreases with increasing temperature. The polarization of domains takes place in two steps; switchable polarization in domain (P_s) and back switched polarization (P_r). When external field is applied, the polarization reaches to its maximum value P_s and when it is withdrawn, the polarization remains P_r . This phenomena is known as back switching polarization (P_{bc}) and its value is given as:

$$P_{bc} = P_s - P_r \quad (5)$$

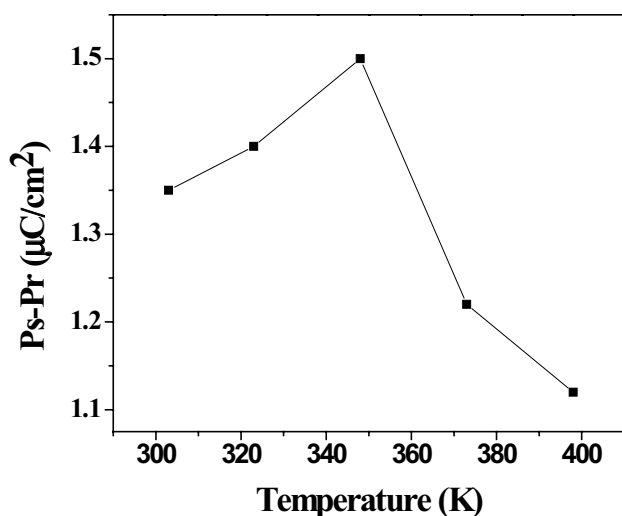


Fig. 10 Plot of back switching polarization ($P_s - P_r$) with temperature at 9 kV/cm electric field

Figure 10 depicts the plot of back switching polarization ($P_s - P_r$) against temperature (T K). The plot indicates that the back switching polarization initially increases with temperature up to 400 K and then decreases signifying the phase transition at 400 K. The back switching polarization also follows the Arrhenius law as given below:

$$P_s - P_r = P_0 \exp\left(\frac{-E_A}{K_B T}\right) \quad (6)$$

where E_A is the average activation energy of trapped charge defect such as oxygen vacancy, and P_0 is a constant. In order to estimate the activation energy involved in the domain switching, the slope of the plot $\ln(P_s - P_r)$ versus $1000/T$ is used (Fig. 11).

4 Conclusions

In this study, the $\text{BaZr}_{0.05}\text{Ti}_{0.95}\text{O}_3$ ceramic is successfully prepared by SSRT. The structural analyses are carried out by XRD and Raman spectroscopy which validate that the material exhibits orthorhombic symmetry. The temperature dependent dielectric behaviour shows the existence of three phase transitions for the present composition. The diffuseness is found to result due to chemical inhomogeneity, and corresponding parameters are obtained from the modified Curie–Wiess law. As an indication of Olsen cycle, it is observed that the present composition would be a suitable candidate for scavenging of waste thermal energy. The ferroelectric scaling relations for coercive field (E_c), remnant polarization (P_r), as a function of temperature (T) are also estimated. The temperature-dependence

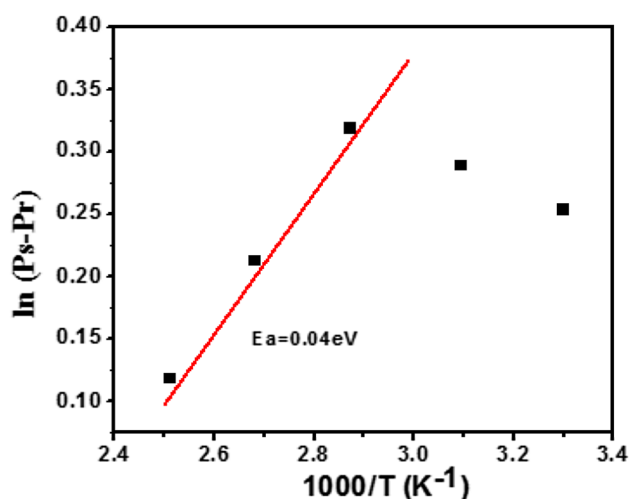


Fig. 11 Plot of $\log(P_s - P_r)$ with $1000/T$ at 9 kV/cm electric field

back-switching kinetics is found to follow the Arrhenius law. The results presented in the manuscript will provide a brief idea about the hysteresis behaviour with temperature under external electric field.

References

- G.H. Haertling, Ferroelectric ceramics: history and technology. *J. Am. Ceram. Soc.* **82**, 797–818 (1999)
- N. Setter, R. Waser, Electroceramic materials. *Acta Mater.* **48**, 151–178 (2000)
- D. Viehland, L. Ewart, J. Powers, J. Li, Stress dependence of the electromechanical properties of $\langle 001 \rangle$ -oriented $\text{Pb}(\text{Mg}_{1/3}\text{Nb}_{2/3})\text{O}_3$ - PbTiO_3 crystals: performance advantages and limitations, *J. Appl. Phys.* **90**, 2479–2483 (2001)
- J. Zhang, Z. Yin, M.S. Zhang, J.F. Scott, Size-driven phase transition in stress-induced ferroelectric thin films. *Solid State Commun.* **118**, 241–246 (2001)
- X.G. Tang, H.L.W. Chan, Effect of grain size on the electrical properties of $(\text{Ba,Ca})(\text{Zr,Ti})\text{O}_3$ relaxor ferroelectric ceramics. *J. Appl. Phys.* **97**, 034109 (2005)
- T.R. Shrout, S.J. Zhang, Lead-free piezoelectric ceramics: alternatives for PZT? *J. Electroceram.* **19**, 113–126 (2007)
- S. Zhang, R. Xia, T.R. Shrout, G. Zang, J. Wang, Characterization of lead free $(\text{K}_{0.5}\text{Na}_{0.5})\text{NbO}_3$ - LiSbO_3 piezoceramic. *Solid State Commun.* **141**, 675–679 (2007)
- Z. Wu, H. Liu, M. Cao, Z. Shen, Z. Yao, H. Hao, D. Luo, Effect of $\text{BaO-Al}_2\text{O}_3\text{-B}_2\text{O}_3\text{-SiO}_2$ glass additive on densification and dielectric properties of $\text{Ba}_{0.3}\text{Sr}_{0.7}\text{TiO}_3$ ceramics. *J. Ceram. Soc. Jpn.* **116**, 345–349 (2008)
- W. Ge, H. Liu, X. Zhao, B. Fang, X. Li, F. Wang, D. Zhou, P. Yu, X. Pan, D. Lin, Crystal growth and high piezoelectric performance of $0.95\text{Na}_{0.5}\text{Bi}_{0.5}\text{TiO}_3$ - 0.05BaTiO_3 lead-free ferroelectric materials. *J. Phys. D* **41**, 115403 (2008)
- S.E. Park, T.R. Shrout, Ultrahigh strain and piezoelectric behaviour in relaxor based ferroelectric single crystals. *J. Appl. Phys.* **82**, 1804–1811 (1997)

11. H. Fu, R.E. Cohen, Polarization rotation mechanism for ultra-high electromechanical response in single-crystal piezoelectrics. *Nature* **403**, 281–283 (2000)
12. J.F. Scott, Prospects for ferroelectrics: 2012–2022. *ISRN Mater. Sci.* **2013**, 187313–187336 (2013)
13. F.H. Schader, E. Aulbach, K.G. Webber, G.A. Rossetti, Influence of uniaxial stress on the ferroelectric-to-paraelectric phase change in barium titanate. *J. Appl. Phys.* **113**, 174103–174111 (2013)
14. J.C. Slater, The Lorentz correction in barium titanate. *Phys. Rev.* **78**, 748 (1950)
15. A.F. Devonshire, XCVI. Theory of barium titanate. *Philos. Mag.* **40**, 1040–1063 (1949)
16. H.D. Megaw, Origin of ferroelectricity in barium titanate and other perovskite-type crystals. *Acta Crystallogr.* **5**, 739–749 (1952)
17. A.V. Hippel, Ferroelectricity: domain structure and phase transitions of barium titanate. *Rev. Mod. Phys.* **22**, 221–237 (1950)
18. B. Matthias, A.V. Hippel, Domain structure and dielectric response of barium titanate single crystals. *Phys. Rev.* **73**, 1378–1384 (1948)
19. W. Cochran, Crystal stability and the theory of ferroelectricity. *Adv. Phys.* **9**, 387–423 (1960)
20. P. Ginet, C. Lucat, F. Ménéil, Modelling and characterizing a screen-printed metallic electrothermal microactuator. *Int. J. Appl. Ceram. Technol.* **4**(5), 423–427 (2007)
21. B.D. Stojanovic, C.R. Foschini, V.B. Pavlovic, V.M. Pavlovic, V. Pejovic, J.A. Varela, Barium titanate screen-printed thick films. *Ceram. Int.* **28**, 293–298 (2002)
22. T. Tick, J. Peränti, H. Jantunen, A. Uusimäki, Screen printed low-sintering-temperature barium strontium titanate (BST) thick films. *J. Eur. Ceram. Soc.* **28**, 837–842 (2008)
23. F. Moura, A.Z. Simoes, B.D. Stojanovic, M.A. Zaghete, E. Longo, J.A. Varela, Dielectric and ferroelectric characteristics of barium zirconate titanate ceramics prepared from mixed oxide method. *J. Alloys Compd.* **462**, 129–134 (2008)
24. G.N. Bhargavi, A. Khare, T. Badapanda, M.S. Anwar, N. Brahme, Electrical characterizations of BaZr_{0.05}Ti_{0.95}O₃ perovskite ceramic by impedance spectroscopy, electric modulus and conductivity. *J. Mater. Sci.: Mater. Electron.* **28**, 16956–16964 (2017)
25. X.P. Jiang, M. Zeng, H.L.W. Chan, C.L. Choy, Relaxor behaviours and tunability in BaZr_(0.35)Ti_(0.65)O₃ ceramics. *Mater. Sci. Eng. A* **438–440**, 198–201 (2006)
26. X.G. Tang, K.H. Chen, H.L.W. Chan, Diffuse phase transition and dielectric tunability of Ba(Zr_yTi_{1-y})O₃ relaxor ferroelectric ceramics. *Acta Mater.* **52**(17), 5177–5183 (2004)
27. A. Mukherjee, P. Victor, J. Parui, S.B. Krupanidhi, Leakage current behaviour in pulsed laser deposited Ba (Zr_{0.05}Ti_{0.95})O₃ thin films. *J. Appl. Phys.* **101**, 034106–034111 (2007)
28. X.G. Tang, Q.X. Liu, Y.P. Jiang, R.K. Zheng, H.L.W. Chan, Enhanced dielectric properties of highly (100) oriented Ba(Zr,Ti)O₃ thin films grown on La_{0.7}Sr_{0.3}MnO₃ bottom layer. *J. Appl. Phys.* **100**, 114105–114109 (2006)
29. R.H. Liang, X.L. Dong, Y. Chen, F. Cao, Y.L. Wang, Dielectric properties and tunability of Ba(Zr_xTi_{1-x})O₃ ceramics under high DC electric field. *Ceram. Int.* **33**, 957–961 (2007)
30. Z. Yu, R. Guo, A.S. Bhalla, Dielectric behaviour of Ba (Ti_{1-x}Zr_x)O₃ single crystals. *J. Appl. Phys.* **88**(1), 410–415 (2000)
31. L. Dong, D.S. Stone, R.S. Lakes, Enhanced dielectric and piezoelectric properties of BaZrO₃-(1-x) BaTiO₃ ceramics. *J. Appl. Phys.* **111**(8), 084107 (2012)
32. A.K. Kalyani, A. Senyshyn, R. Ranjan, Polymorphic phase boundaries and enhanced piezoelectric response in extended composition range in the lead free ferroelectric BaTi_{1-x}Zr_xO₃. *J. Appl. Phys.* **114**, 014102 (2013)
33. A.G. Serrano, A.L. Bonaventura, J.R. Boschilia, E. Antonelli, Microstructural, structural and electrical properties of bilayered BaZr_{0.05}Ti_{0.95}O₃/Ba_{0.75}Sr_{0.25}TiO₃. *Mater. Res. Bull.* **87**, 34–39 (2017)
34. Y. Tan, J. Zhang, Y. Wu, C. Wang, V. Koval, B. Shi, H. Ye, R. McKinnon, G. Viola, H. Yan, Unfolding grain size effects in barium titanate ferroelectric ceramics. *Sci. Rep.* **5**, 9953 (2015)
35. N. Yasuda, H. Ohwa, S. Asano, Dielectric properties and phase transitions of BaTi_{1-x}Sn_xO₃ Solid solution. *Jpn. J. Appl. Phys.* **35**(1), 5099–5103 (1996)
36. Y. Shiratori, C. Pithan, J. Dornseiffer, R. Waser, Raman scattering studies on nanocrystalline BaTiO₃ Part I—isolated particles and aggregates. *J. Raman Spectrosc.* **38**, 1288–1299 (2007)
37. F.M. Pontes, M.T. Escote, C.C. Escudeiro, E.R. Leite, E. Longo, A.J. Chiquito, P.S. Pizani, J.A. Varela, Characterization of BaTi_{1-x}Zr_xO₃ thin films obtained by a soft chemical spin-coating technique. *J. Appl. Phys.* **96**, 4386–4391 (2004)
38. A. Dixit, S.B. Majumder, P.S. Dobal, R.S. Katiyar, A.S. Bhalla, Phase transition studies of sol-gel deposited barium zirconate titanate thin films. *Thin Sol. Films* **447**, 284–287 (2004)
39. P.S. Dobal, A. Dixit, R.S. Katiyar, Z. Yu, R. Guo, A.S. Bhalla, Phase transition behaviour of BaZr_xTi_{1-x}O₃ ceramics. *J. Raman Spectrosc.* **32**, 69–71 (2001)
40. T. Badapanda, S. Sarangi, B. Behera, P.K. Sahoo, S. Anwar, T.P. Sinha, G.E. Luz Jr., E. Longo, L.S. Cavalcante, Structural refinement, optical and ferroelectric properties of microcrystalline Ba(Zr_{0.05}Ti_{0.95})O₃ perovskite. *Curr. Appl. Phys.* **14**, 708–715 (2014)
41. K. Wagner, The theory of a heterogeneous dielectric. *Annu. Phys.* **40**, 817–855 (1913)
42. C. Koops, On the Dispersion of resistivity and dielectric constant of some semiconductors at audio frequencies. *Phys. Rev.* **83**, 121–124 (1951)
43. S. Chougule, B. Chougule, Studies on electrical properties and the magnetoelectric effect on ferroelectric-rich (x) Ni_{0.8}Zn_{0.2}Fe₂O₄(1-x) PZT ME composites. *Smart Mater. Struct.* **16**, 493–497 (2007)
44. B. Tareev, *Physics of dielectric materials* (MIR Publications, Moscow, 1979)
45. D.W. Richerson, *Modern ceramic engineering: properties, processing, and use in design*, 2nd edn. (Marcel Dekker, New York, 1992)
46. G. Yao, X. Wang, Y. Zhang, Z. Shen, L. Li, Nb-Modified 0.9BaTiO₃-0.1(Bi_{0.5}Na_{0.5})TiO₃ ceramics for X9R high-temperature dielectrics application prepared by coating method. *J. Am. Ceram. Soc.* **95**, 3525–3531 (2012)
47. S.J. Kuang, X.G. Tang, L.Y. Li, Y.P. Jiang, Q.X. Liu, Influence of Zr dopant on the dielectric properties and Curie temperatures of Ba(Zr_xTi_{1-x})O₃ (0 ≤ x ≤ 0.12) ceramics. *Scr. Mater.* **61**, 68–71 (2009)
48. Y.W. Li, X.L. Zhou, F.X. Li, Temperature-dependent mechanical depolarization of ferroelectric ceramics. *J. Phys. D* **43**(17), 175501 (2010)
49. T. Maiti, R. Guo, A.S. Bhalla, Evaluation of experimental resume of BaZr_xTi_{1-x}O₃ with perspective to ferroelectric relaxor family: an overview. *Ferroelectrics* **425**(1), 4–26 (2011)
50. R.B. Olsen, D.A. Bruno, J.M. Briscoe, Pyroelectric conversion cycles. *J. Appl. Phys.* **58**, 4709–4716 (1985)
51. R. Olsen, D. Bruno, Pyroelectric conversion materials. In *IECEC '86; Proceedings of the Twenty-first Intersociety Energy Conversion Engineering Conference*, San Diego (1986), pp. 89–93
52. I.M. McKinley, R. Kandilian, L. Pilon, Waste heat energy harvesting using the Olsen cycle on 0.945Pb(Zn_{1/3}Nb_{2/3})O₃-0.055PbTiO₃ single crystals. *Smart Mater. Struct.* **21**(3), 035015 (2012)
53. F.Y. Lee, S. Goljahi, I.M. McKinley, C.S. Lynch, L. Pilon, Pyroelectric waste heat energy harvesting using relaxor ferroelectric

- 8/65/35 PLZT and the Olsen cycle. *Smart Mater. Struct.* **21**(2), 025021 (2012)
54. S. Alpay, J. Mantese, S. Trolier-McKinstry, Q. Zhang, R.W. Whatmore, Next-generation electrocaloric and pyroelectric materials for solid-state electrothermal energy interconversion. *MRS Bull.* **39**(12), 1099–1111 (2014)
55. S. Patel, A. Chauhan, R. Vaish, Enhanced energy harvesting in commercial ferroelectric materials. *Mater. Res. Express* **1**, 025504 (2014)
56. R. Yimnirun, A. Ngamjarurojana, R. Wongmaneerung, S. Wongsanmai, S. Ananta, Y. Laosiritaworn, Temperature scaling of ferroelectric hysteresis in hard lead zirconate titanate bulk ceramic. *Appl. Phys. A* **89**(3), 737–741 (2007)
57. R. Yimnirun, R. Wongmaneerung, S. Wongsanmai, A. Ngamjarurojana, S. Ananta, Y. Laosiritaworn, Temperature scaling of dynamic hysteresis in soft lead zirconate titanate bulk ceramic. *Appl. Phys. Lett.* **90**(11), 112906–112913 (2007)
58. S. Patel, A. Chauhan, R. Vaish, Electrocaloric behaviour and temperature-dependent scaling of dynamic hysteresis of $\text{Ba}_{0.85}\text{Ca}_{0.15}\text{Ti}_{0.9}\text{Zr}_{0.1}\text{O}_3$ ceramics. *Int. J. Appl. Ceram. Technol.* **12**(4), 899–907 (2015)
59. R. Yimnirun, S. Wongsanmai, R. Wongmaneerung, N. Wongdamnern, A. Ngamjarurojana, S. Ananta, Y. Laosiritaworn, Stress and temperature-dependent scaling behaviour of dynamic hysteresis in soft PZT bulk ceramics. *Phys. Scr.* **129**, 184–189 (2007)
60. X. Chen, X. Dong, H. Zhang, N. Feng, H. Nie, F. Cao, G. Wang, Y. Gu, H. He, Temperature scaling of dynamic hysteresis in Zr-rich $\text{PbZr}_{1-x}\text{Ti}_x\text{O}_3$ ceramics. *J. Appl. Phys.* **105**, 096104 (2009)